Robotica (2002) volume 20, pp. 181–193. © 2002 Cambridge University Press
DOI: 10.1017/S0263574701003770 Printed in the United Kingdom

Velocity, acceleration and deceleration bounds for a time-optimal planner of a wheeled mobile robot

María Prado, Antonio Simón and Francisco Ezquerro

Department of Mechanical Engineering, University of Málaga, Plaza El Ejido s/n, 29013 Málaga (Spain)
E-mail: mpn@uma.es

(Received in Final Form: September 19, 2001)

SUMMARY
Three single-valued upper boundary functions for velocity, acceleration and deceleration of a wheeled mobile robot (WMR) are defined as closed mathematical forms over its entire spatial path. The limits deal with mechanical, kinematic and dynamic characteristics of the robot and with task and operating matters. These boundary functions can be computed making use of any robot model, as complex as is needed, since it works offline.

All studies are particularised for the robot RAM. A kinematic and a complete dynamic model of this WMR is built, with special attention on the study of wheel-ground contact efforts. For this purpose an empirical-analytical model of rubber wheel rolling is developed.

KEYWORDS: Mobile robots; Time-optimal motion planning; Velocity boundary; Acceleration boundary; Dynamic robot models

1. INTRODUCTION

The control system of WMRs generally comprises two different modules: a trajectory planner and a trajectory tracking controller. Frequently the trajectory planner works under path-velocity decomposition,[1] i.e. it divides its task into two consecutive stages: spatial-planning (SP), involving the definition of a continuous function of robot positions in the environment from the starting point to the goal point; and temporal-planning (TP), which involves building a velocity profile for the spatial path.

Many SP methods which look for the shortest spatial path and use smooth curves that satisfy the curvature continuity have been addressed in previous works.[2] But most of them do not take into account any consideration regarding velocity, acceleration or deceleration bounds.

Apart from the solution process followed for the first task, the generation of a good velocity profile is crucial in generating a time-optimal trajectory. Moreover, simply in the planning of a good trajectory it is imperative at least to attend to the kinematics and dynamics of the robot guide point velocity as well as its first derivative.[3]

This paper identifies the constraints that condition the maximum velocity, acceleration and deceleration of a WMR searching for the fastest trajectory, but also demanding the trajectory to be:

- Feasible: which makes it necessary to study the kinematics and dynamics of the robot, in addition to constructive characteristics of its mechanical subsystems.
- Safe: avoiding the planning of velocities or accelerations that lead to dangerous motions.
- High precision tracking: the spatial error, which is the position error between the planned spatial path and the tracked one, and the temporal error, time gap between the moment at which it is estimated to arrive at a position and the moment in which it is reached, are bounded.
- Low computational cost: in order to be included in real-time planners, the boundary functions are always closed mathematical forms.

From all the constraints, three upper boundary functions for velocity, acceleration and deceleration are generated, which are single-valued over the entire spatial path domain.

To search lower boundary functions for velocity and acceleration does not make sense in time-optimal planning, since the maximum feasible velocity should always be chosen.

This paper tests the success of the proposed boundary functions by incorporating them in the TP stage of the trajectory planner of a WMR that works following path-velocity decomposition. But they can also be used by any other approach to the planning problem: to improve the upper limits when the planner uses intelligent strategies to bound wheel velocities or accelerations;[4] as a previous stage for trajectory planners that integrate SP and TP considering an upper limit for velocity, as Ramírez[5] has done, but where the velocity upper limit is simply an arbitrary constant and nothing is done about the robot's acceleration and deceleration

To our knowledge, the first references addressing trajectory planning with kinematic and dynamic constraints for WMR are those of O'Dunlaing[6] and Fujimura.[7] These papers, as a number of other algorithms to solve the TP stage,[8] are based on constant maximum values for robot velocity and acceleration, set to arbitrary constants which are unrelated to the mechanical characteristics of the system.

Other recent works seek to find a way how to fix upper bounds for those operating variables, but never in a global way and always based on simplified dynamic robot models which are directly included in the trajectory planner.

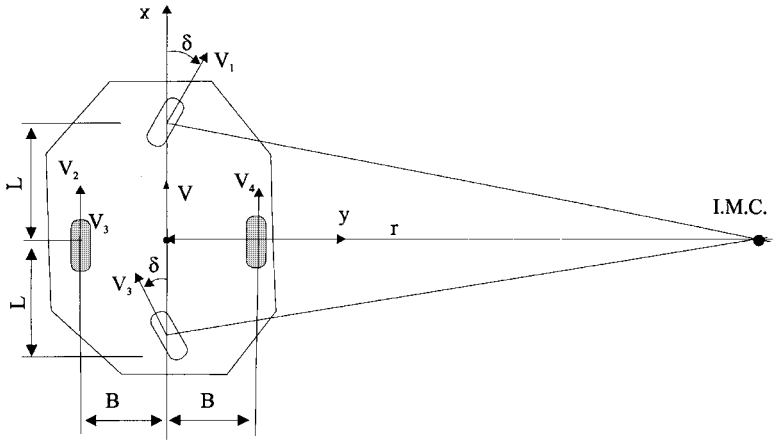

Fig. 1. RAM's mechanical configuration.

Weiguo[9] proposes a velocity profile planner for WMRs on flat and homogeneous terrains, where velocity and acceleration are limited by the outer motor torques and by the absolute slippage of the vehicle on the ground. Choi[10] develops another planner where velocity and acceleration are constrained by dynamic characteristics related to the performance of the robot's electric motors and its battery's power.

Some other limitations have been studied mainly within the framework of projects for planetary exploration. Shiller[11] deals with some dynamic constraints: sliding restrictions, also understood as the avoidance of absolute vehicle slippage, tip-over and loss of wheel-ground contact constraints, important subjects on irregular outdoor terrains. The author works with a very simplified robot model, neglecting sideslip and assuming pure rolling, so wheel deformations and microslippages which can cause important tracking errors are not quantified. Cheriff[12] also proposes a set of kinematic and dynamic constraints over the robot path, dealing specifically with 3D irregular and non-homogeneous grounds. The resulting trajectory planner directly incorporates a complete dynamic WMR model, considering non-linear motions and accounting specifically for wheel-ground interactions, which makes it necessary to run complex algorithms that significantly increase computational cost. Perhaps for this reason the author applies a simplified model to the contact efforts calculation: forces are evaluated by piecewise linear functions, separating the lateral force from the longitudinal one and neglecting the slip angle in steering wheels. Finally, the paper develops a trajectory planner that takes constraints for robot velocity in account, based on a maximum arbitrary value which is not fixed in the paper, and for robot acceleration and deceleration, based on the motor's torque and adhesion restrictions.

This paper addresses mainly the TP problem in indoor environments, so flat terrains are considered and robot motion is developed on 2D grounds. However, considering non-zero grades can be done simply by including a vectorial grade in the calculation of the normal and tangential forces in the tip-over constraint and, on the other hand, by retaining the variable j in dynamic constraints and in constraints which are forced by the ground for acceleration and deceleration.

For the same reason, only homogeneous surfaces are dealt with, but other cases can be included effortlessly by handling the wheel-ground friction coefficient, μ, not as a constant but as a known function along the spatial path.

Additionally, the bounds do not deal explicitly with mobile environments, but they can easily be extended to include moving obstacles, as explained in Section 3.4.

The paper is organised as follows: In Section 2, the planning problem is defined for the WMR RAM, which is briefly described there, as well as its kinematic and dynamic model; this is the robot where the constraints will be implemented. Next, the bounds for velocity, in Section 3, and for acceleration and deceleration, in Section 4, are identified, all of them particularised for RAM. In Section 5, the restrictions are summed up in three single-valued boundary functions extended over the entire path domain. In order to test the work, Section 6 presents the boundary functions found for RAM in a dynamic hard path. Finally, Section 7, summarises the conclusions of the paper.

2. THE ROBOT RAM

RAM is a WMR designed for navigation with high manoeuvrability in indoor and outdoor industrial environments.[13] Its mechanical configuration consists of four wheels located at the vertices of a rhombus, one of whose diagonals is the longitudinal axis of the vehicle (see Figure 1). The two lateral wheels, wheels 2 and 4, are a semi-track B away from RAM's geometric centre and are centred on the longitudinal axis of the robot, they are driven and unsteered parallel wheels. The front and rear wheels, wheels 1 and 3, are a semi-wheelbase L away from RAM's geometric centre and are centred on its transverse axis, they are steering wheels. Completely independent servomechanisms power the two driven wheels. The two steering wheels are linked by a mechanical system that imposes steering angles of equal magnitude and opposite sign on both.

Since the robot is only expected to have to negotiate small grades, it simply builds in suspension systems at the two

https://doi.org/10.1017/S0263574701003770 Published online by Cambridge University Press

lateral wheels. These are two independent spring/damper sets in parallel configuration.

Braking effort is applied on the axis of the tractive servomotors by an electromechanical brake. Thus, only the driven wheels are braking wheels for RAM, and the braking force is all or nothing.

The guide point is positioned at the centre of the non-steered lateral axis, which coincides with the robot's centre of gravity (c.g.) and with its geometric centre in plan view.

The trajectory planner of RAM works on three levels, in the same way as most WMR trajectory planners that employ path-velocity decomposition. First of all, its global planner finds a route, a set of postures in the environment that must be reached sequentially by the robot guide point. Then the SP is addressed, task which involves restrictions exclusively related to the configuration parameter of the robot and its derivatives, mainly non-holonomic constraints, and therefore it works under the solution of the direct kinematic problem. Next the TP is dealt with by appending a velocity profile to the spatial path; in this stage, time-dependent limits for velocity and acceleration must be taken in account. And finally, in order for this trajectory to be tracked, the robot generator will calculate the reference functions for the control variables, under the solution of the inverse kinematic problem.

2.1. Kinematic robot model

When solving the kinematic problem of RAM, a world frame with X and Y axis on ground plane, $\mathcal{F}w$, and a local coordinate system attached to the guide point of the robot, $\mathcal{F}\ell$, shown in Figure 2, are employed. The internal coordinates are the angular velocities of the driven wheels around their rotational axis, ω_2 and ω_4, and the steering angle, δ. Meanwhile, as external coordinates, the guide point linear velocity on ground, V, and the curvature of its trajectory, κ, are chosen. Thus, the inverse kinematic solution, when R is the wheel radius, is given by the system:

$$\omega_2 = \frac{V}{R}(1+\kappa B)$$

$$\omega_4 = \frac{V}{R}(1-\kappa B) \qquad (1)$$

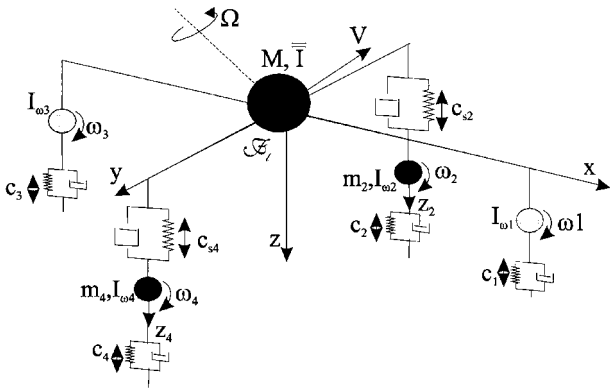

Fig. 2. RAM's dynamic model.

$$\delta = \text{atan}(L\kappa)$$

If [X, Y] is the position of $\mathcal{F}\ell$ with respect to (w.r.t.) $\mathcal{F}w$, assuming flat ground which makes Z a constant, and if θ is the heading of $\mathcal{F}\ell$ w.r.t. $\mathcal{F}w$, then the direct kinematic solution, parameterised by the arc length, s, is expressed by:

$$\theta(s) = \theta(s_0) + \int_{s_0}^{s} \kappa ds$$

$$X(s) = X(s_0) + \int_{s_0}^{s} \cos(\theta) ds \qquad (2)$$

$$Y(s) = Y(s_0) + \int_{s_0}^{s} \sin(\theta) ds$$

2.2. Dynamic robot model

The dynamic model of RAM[14] is developed dealing with suspension systems and paying very especial attention to the efforts in rubber wheel-ground interaction, developing a specific analytical-empirical model.

The robot's dynamics are analysed employing the coordinate systems $\mathcal{F}w$ and $\mathcal{F}\ell$.

A. Modelling the robot multibody. The robot is modelled as three concentrated masses: a mass M located at the c.g. of the sprung mass and with matrix of mass moment of inertia $\bar{I}$; two masses, $m_{ss} = [m_2\ m_4]^t$, located at the c.g. of the two semi-sprung masses.[15] M has six degrees of freedom (dof) expressed by its linear velocity, $\vec{V}$, with three orthogonal components $[V_x\ V_y\ V_z]$ in $\mathcal{F}\ell$, and its angular velocity $\vec{\Omega}$, as $[\Omega_x, \Omega_y, \Omega_z]$ in the same reference. While the motions of m_2 and m_4 are restricted to the displacement relative to M in the direction of the z axis of $\mathcal{F}\ell$, their relative velocities are $z = [z_2\ z_4]^t$. Finally, there are four other masses located at the geometric centre of each wheel, whose only dof is its angular velocity around the wheel's axis, $\omega = [\omega_1\ \omega_2\ \omega_3\ \omega_4]$, and with moment of inertia $I_\omega = [I_{\omega1}\ I_{\omega2}\ I_{\omega3}\ I_{\omega4}]$.

Each suspension system between M and m_{ss} is modelled by a spring-damper set in the direction of the relative motions.

Regarding the rubber wheels, their behaviour in normal direction to the ground, is modelled as a spring-damper with constant coefficients,[15] while the efforts in the tangential direction are studied in Section B. The complete WMR model, as well as the state variables for simulation, are depicted in Figure 2.

By analytical mechanics laws, the motion of the sprung mass on the $\mathcal{F}\ell$ fame, neglecting the aerodynamic actions, is given by the differential system:

$$\vec{F}_g + \vec{F}_s^n + \vec{F}_{w_{ns}}^n + \vec{F}_w^t = M\dot{\vec{V}} + M\vec{\Omega}x\vec{V} \qquad (3)$$

where $\vec{F}_g$ is the gravity force, $\vec{F}_s^n = [\vec{F}_{s2}^z\ \vec{F}_{s4}^z]$ are the forces from the two suspensions in the direction of the local axis z, $\vec{F}_{w_{ns}}^n = [\vec{F}_{w1}^{z_1}\ \vec{F}_{w3}^{z_3}]$ are the forces normal to the ground from the treads of wheels 1 and 3 linked to M without suspension, and $\vec{F}_w^t$ are the forces tangential to the ground from the treads of all the wheels. Equation (3) assumes that the robot's roll and pitch angles are small, hence they can be neglected when the action of the ground contact efforts on the sprung mass is studied.

https://doi.org/10.1017/S0263574701003770 Published online by Cambridge University Press

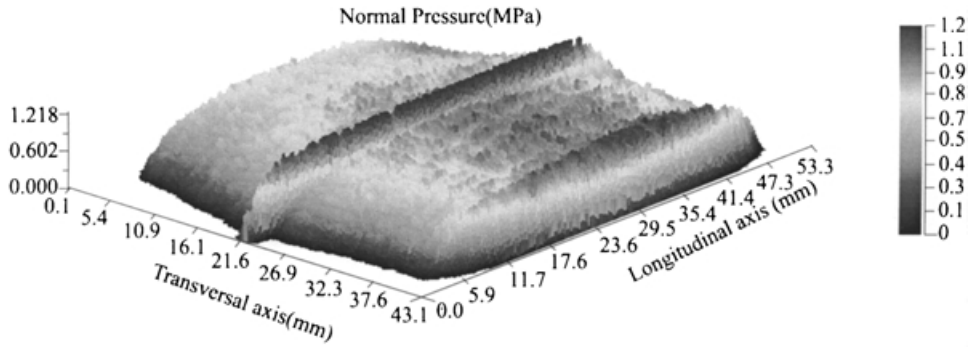

Fig. 3. Measurement of the normal pressure distribution at the contact area of the wheels of RAM.

On the other hand, the rotational motion of M is expressed by:

$$\vec{T}_s^n+\vec{T}_{w_{ns}}^n+\vec{T}_w^t=\bar{I}\dot{\vec{\Omega}}+\vec{\Omega}x(\bar{I}\vec{\Omega}) \quad (4)$$

where $\vec{T}_i^j$ is the torques acting over M derived from the forces marked with the same notation as in the expression (Equation 3).

The motion of the two unsprung masses is given by:

$$m_{ss}z=F_s^n+F_{w_s}^n \quad (5)$$

where $F_{w_s}^n=[F_{w2}^{z_2}\ F_{w4}^{z_4}]^t$ is the column vector of the forces at the wheels with suspensions in direction normal to the ground.

Regarding the spring-dampers that model the suspensions, calling the distance from wheels 2 and 4 to M in the direction of the j axis of $\mathcal{F}\ell$ $dj=[d_{j,2}\ d_{j,4}]^t$, the compression at the two suspension systems $c_s=[c_{s2}\ c_{s4}]^t$ follows the differential equation:

$$\dot{c}_s=V_z+d_x\Omega_x \quad (6)$$

And the compression at the spring-dampers that model the wheels, $c_r=[c_{r1}\ c_{r2}\ c_{r3}\ c_{r4}]$, where hs_i is the vertical profile of the ground at the i-th wheel, is, respectively for wheels with or without suspension:

$$[\dot{c}_{r1}\ \dot{c}_{r3}]^t=V_z+[d_{x,1}\ d_{x,3}]^t\Omega_y+[\dot{hs}_1\ \dot{hs}_3]^t \quad (7)$$

$$[\dot{c}_{r2}\ \dot{c}_{r4}]^t=z+[\dot{hs}_2\ \dot{hs}_4]^t$$

Finally, the angular velocity of the wheels[16] is:

$$I_\omega\dot{\omega}=T_T+F_w^x(R-c_r)-F_w^n\Delta_x-c_\varphi\omega-\phi_{pr} \quad (8)$$

where T_T is the column vector of tractive or braking torques at the four wheel axis, F_w^x is the column vector of the contact forces at the wheel treads in their longitudinal direction, R is wheel radius, Δ_x is the column vector of the amount of longitudinal offset of centre of vertical pressure from wheel centres, c_ω is the column vector of the wheel damping coefficient and ϕ_{rp} is the column vector of passive resistance torques. δ_x and c_ω are habitually neglected, in most vehicular dynamics, and ϕ_{rp} can be equal to zero for non-driven wheels.

Thus a system of eighteen first-order non-linear differential equations, (3), (4), (5), (6), (7) and (8), describes the movements of RAM. This model was validated successfully.[14]

B. Modelling rubber wheel-ground interaction. A physical model of wheel-ground contact for uniform rubber wheels without profile is developed from the Fiala hypothesis for pneumatic tyres,[16] but considering for this case that:

(i) The normal pressure in the contact area of the wheels follows the Hertz distribution in the longitudinal direction and is uniform, in the transversal direction. These hypotheses were validated experimentally,[17] as shown in Figure 3.

(ii) The direction of the tangential stress at any sliding point of the wheel tread is imposed by the stress at the point of the tread where the adhesion capability is saturated. This hypothesis was validated[14] using the experimental results found for tyres.[18]

The wheel tread is assumed to be a rectangular area, approximated experimentally,[17] where two different zones are studied (see Figure 4):

(a) Sticking zone: it is always at the front of the tread. The tangential stress is a function of the rubber deformation, $\vec{\varepsilon}$, given by:

$$\vec{\tau}^{\,stick}=\vec{k}_{rub}\vec{\varepsilon}=\vec{k}_{rub}\vec{d}\ x^w \quad (9)$$

where $\vec{k}_{rub}$ is the rubber elastic stiffness, $\vec{d}$ is the slip vector and x^w is the distance from the point of the wheel tread to its touchdown point. In sticking, the slip vector is the ratio between the slip velocity and the longitudinal velocity of the wheel, and can be expressed as a function of the longitudinal slip of the wheel, i, and its slip angle, α, by:

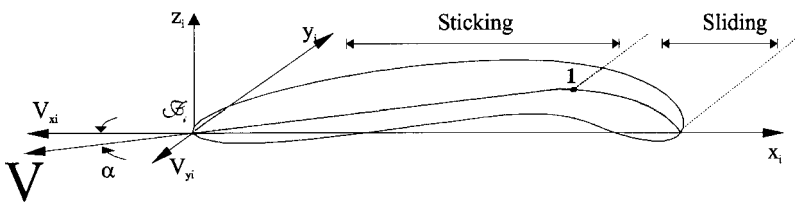

Fig. 4. Model for the rubber wheel-ground interaction.

https://doi.org/10.1017/S0263574701003770 Published online by Cambridge University Press

$$\vec{d} = \frac{\vec{v}_s}{v_1} = [i \tan(\alpha)]^t \quad (10)$$

(b) Sliding zone: it is always at the rear of the tread and it can be null, shorter or equal to the tread length. The magnitude of the tangential stress is given by the Coulomb friction law and its direction follows the hypothesis 2 mentioned previously. So when σ_n is the normal pressure, in accordance with hypothesis 1:

$$\vec{\tau}^{\,slip} = \mu\sigma_n \frac{\vec{k}_{rub}\vec{d}}{|\vec{k}_{rub}\vec{d}|} \quad (11)$$

The point where the adhesion ability of the wheel is saturated, the transition between the sticking and the sliding zone, is at a distance of x_1^w from the touchdown point of the tread, found as:

$$|\vec{\tau}^{\,skip}(x_1^w) = \mu\sigma_n(x_1^w) \quad (12)$$

Integrating the tangential stress given by equations (9) and (11) over the entire tread, the contact force is given by:

$$\vec{F}_w^t = \frac{\vec{C}\vec{d}}{4}\left[2\lambda + \sqrt{\frac{\lambda}{1-\lambda}}\left(\frac{\pi}{2} + \text{asin}\,(1-2\lambda)\right)\right] \quad \ldots\ldots \lambda < 1 \quad (13)$$

$$\vec{F}_w^t = \vec{C}\vec{d} \quad \ldots\ldots \lambda = 1$$

where $\vec{C}$ is the wheel stiffness vector that groups the longitudinal and the cornering stiffness of the wheel:

$$\vec{C} = [C_s\ C_\alpha]^t = \left[\left.\frac{dF_w^x}{ds}\right|_{\vec{d}=[0\,0]} \left.\frac{dF_w^y}{d\alpha}\right|_{\vec{d}=[0\,0]}\right]^t \quad (14)$$

And $\lambda = x_1^w/l$ is the ratio of the sticking length w.r.t. the total length of the wheel, l, computed as:

$$\lambda = \mu\frac{F_w^n}{2}\frac{1}{|\vec{C}\vec{d}|} \quad (15)$$

3. VELOCITY CONSTRAINTS

This section deals with constructive characteristics, kinematic configuration and dynamic behaviour of a WMR, as well as operational matters, in order to identify the constraints that influence its maximum velocity. All work is particularised for RAM.

3.1. Constructive constraints

Thermal and mechanical characteristics of electric motors and batteries impose their maximum rotational velocities, ω_t^{max} and ω_s^{max}, on the tractive and steering servomotors, respectively.[10]

So, if ξ_t is the reduction ratio of the drive-train, the maximum linear velocity of driven wheels on the ground should never be higher than:

$$v_w^{max} = \xi_t\omega_t^{max}R \quad (16)$$

On the other hand, calling the velocity of variation of the steering angle G_s, its maximum should be:

$$G_s^{max} = \xi_s\,|\,\omega_s^{max}\,| \quad (17)$$

where ξ_s is the reduction ratio of the steering-train.

3.2. Kinematic constraints

In the previous section, the robot's constructional characteristics established the performance of its powered wheels, now they will determine the behaviour of the robot's guide point. First of all, attending to kinematic linkages between the driven wheels and the guide point, the velocity of the latter finds an upper bound in:

$$V_{lim1} = v_w^{max}\frac{|\,1/\vec{\kappa}\,|}{|\,1/\vec{\kappa} + \vec{d}_t^{max}\,|} \quad (18)$$

where $\vec{d}_t^{max}$ is the position vector of the most distant driven wheel w.r.t. the guide point.

Next, by considering kinematic linkages between the steering wheels and the guide point, a second boundary function is found for the velocity of the latter as:

$$V_{lim2} = \frac{|\,d\kappa/dt\,|}{|\,d\kappa/ds\,|} \quad (19)$$

The absolute value frees the constraint from the rotational direction of the trajectory. The numerator will be calculated from the kinematic model of the vehicle, whereas the denominator is directly computed from the known spatial path.

For RAM, both previous bounds, expressions (18) and (19), yield:

$$V_{lim1}^{RAM} = \xi_t\omega_t^{max}\,R\,\frac{1}{1+|\,\vec{\kappa}\,|\,B} \quad (20)$$

$$V_{lim2}^{RAM} = \xi_s\,|\,\omega_s^{max}\,|\,\frac{1+L^2\kappa^2}{L}\frac{1}{|\,d\vec{\kappa}/ds\,|} \quad (21)$$

3.3. Dynamic constraints

In the two first points of this section, a dynamic model of the robot which is as complex as needed for successful results is used to generate offline boundary functions, which are integrated in the planner algorithm in an effective way. Therefore, it is possible to use a robot model which is not limited by its dof, geometric non-linearities, integration tolerances, etc . . .

The resulting velocity limits are related to the sliding constraint proposed by previous works[9,11,12] but not only is total vehicle slippage avoided, which is caused by high wheel deformations and the total expansion of micro-slippage in the wheel-ground contact area, but also deformations and microslippages previous to the total slippage are bounded, in order to reduce spatial and temporal errors of the WMR tracking the trajectory.

A. Maximum velocity to bound the spatial error. Let the quadratic spatial error of a mobile robot be the square of the distance from the actual position of its guide point tracking a trajectory, to the position planned by the spatial path

https://doi.org/10.1017/S0263574701003770 Published online by Cambridge University Press

generator, measured on the ground plane and parameterised by the normalised arc length, i.e. the ratio of s to the total path length, $\hat{s}=s/S$. This is the position error of the real robot tracking the trajectory w.r.t. a virtual target vehicle.[4]

The planned spatial path is expressed, on $\mathcal{F}w$, as:

$$TR_p=[X, Y]:\ [0, 1]\rightarrow\Re^2 \tag{22}$$

This function is generated very frequently, making use of the kinematic problem solution, as stated in Section 2, therefore neglecting the robot side-slip angle, β. However, in general, β takes non-zero values when the trajectory is tracked.

Let the real trajectory be expressed by another two dimensional function on $\mathcal{F}w$, TR_r, as:

$$TR_r=[X_\beta, Y_\beta]:\ [0, 1]\rightarrow\Re^2 \tag{23}$$

Then, the quadratic spatial error can be calculated by:

$$E_s^2(\hat{s})=\sqrt{(X(\hat{s})-X_\beta(\hat{s}))^2+(Y(\hat{s})-Y_\beta(\hat{s}))^2} \tag{24}$$

Now, let the total quadratic spatial error, TE_s, be the integral of E_s[19] all over the path, as:

$$TE_s^2(\hat{s})=\int_0^1 E_s^2(\hat{s})d\hat{s} \tag{25}$$

If TR_p is particularised for stationary trajectories, i.e. with constant velocity and curvature, and the starting point is set at the origin of $\mathcal{F}w$, with no effect on the generality of the problem, the kinematics of RAM, under equation (1), yields:

$$TR_p(\hat{s})=\left[\frac{\sin(2\pi\hat{s})}{\kappa}, \frac{1}{\kappa}(1-\cos(2\pi\hat{s}))\right] \tag{26}$$

On the other hand, when sideslip β is not neglected, calling the real tracked curvature κ^{real}, the real trajectory of the robot is (see Figure 5):

$$TR_r(\hat{s})=\left[\frac{1}{\kappa^{real}}[\sin(\beta+2\pi\hat{s})-\sin(\beta)], \frac{1}{\kappa^{real}}[\cos(\beta)-\cos(\beta+2\pi\hat{s})]\right] \tag{27}$$

The real trajectory can be approximated by the trajectory obtained as simulation output of a sufficiently accurate dynamic model. Then, if the dynamic simulation outputs are marked by the subscript d:

$$\kappa^{real}=\kappa_d \qquad \beta=\beta_d \tag{28}$$

Simulation outputs of the RAM's dynamic model in Section 2.2. allow for the computation of κ_d as a linear function of the guide point velocity, given by:

$$\kappa_d=a_1\kappa \quad ; \quad a_1=1 \tag{29}$$

Thus, the real trajectory curvature is very approximately the one calculated according to the robot's kinematics.

The same conclusion will be reached for all WMRs characterised by neutral steer behaviour. This occurs when the quotient between the cornering stiffness of any wheel, C_α, and the static weight that it supports, is almost constant and, in addition, when the variation range of C_α can be neglected. The first condition is verified for any whose wheels are all identical and when the weight on each one of them is uniform. The second one is accepted when the slip angle is lower than 4° approximately, which happens in trajectories with lateral acceleration up to approximately 0.3g for pneumatic or rubber wheels.[19, 20]

The same simulation results make it possible to express the sideslip angle of the robot as:

$$\cos(\beta_d)=\sqrt{1-(a_2V\kappa)^2}; \quad a_2=5.23\cdot10^{-2} \tag{30}$$

Thus, when the mobile robot RAM navigates a whole stationary circle, by replacing equations (26) and (27) in equation (25), and considering the simulation results of equations (29) and (30) the total spatial error results in:

$$TE_s^2=4\frac{1-\sqrt{1-(a_2V\kappa)^2}}{k^2} \tag{31}$$

The velocity planner fixes an upper bound for this value characteristic of each posture, with its own operating magnitudes $\{V, \kappa\}$. Even knowing that in general the operating variables do not stay constant at adjacent postures, it is understood that they will experience smooth variations since smooth trajectories are pursued. Moreover, many times the spatial path is generated as a piecewise constant curvature function (for example curve type CSC[12]). Therefore, it is understood that the error at each posture can be computed as a function of the error found considering

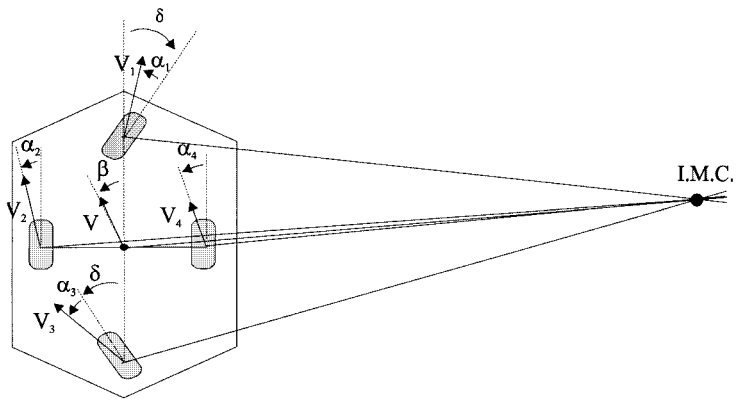

Fig. 5. Tracked trajectory with β not zero.

https://doi.org/10.1017/S0263574701003770 Published online by Cambridge University Press

neighbourhoods where the operating variables stay constant.

This method bounds the total quadratic spatial error by a magnitude relative to the total quadratic spatial error exclusively associated with curvature changes. If t_s^{rel} is the allowed percentage of reduction of the trajectory radius for any mobile robot, the following inequality should be true:

$$TE_s^2 \leq \frac{\pi}{\kappa^2}(1-(t_s^{rel})^2) \tag{32}$$

When the constraint is applied to the result calculated in equation (31) for RAM, a new boundary function for the robot velocity is obtained as:

$$V_{Lim3} = \frac{1}{a_2\kappa}\sqrt{\frac{\pi}{2}t_s^{rel}(2-t_s^{rel})\left(1-\frac{\pi}{8}t_s^{rel}(2-t_s^{rel})\right)} \tag{33}$$

That is, the velocity must be inversely proportional to the planned curvature, as was to be expected, where the proportionality constant is a function of a parameter, a_2, that must be obtained, offline, from an accurate robot dynamic model.

B. Maximum velocity to bound the temporal error. When a WMR is navigating, not only position error must be taken into account, but temporal error can also be important if fitting or synchronising several objects is desired. Let the temporal error of a WMR be the time gap between the real instant when the robot arrives at a posture, t^{real}, and the instant when the path tracker under the robot kinematic model computes it should be reaches, t^{kin}:

$$E_t = t^{real} - t^{kin} \tag{34}$$

For a stationary trajectory of length S, calling the real velocity of the robot V^{real} and the velocity computed by the path tracker under the solution of the direct kinematic problem V, this error is:

$$E_t = S\left(\frac{1}{V^{real}} - \frac{1}{v}\right) \tag{35}$$

The error is mainly due to not pure rolling of real wheels, where elastic deformations and slippage or microslippage occur, effects that are summed up in the longitudinal slip of the wheel, neglected by kinematics. Moreover, these phenomena can not be detected by odometric sensorial systems, which are usually employed by the path trackers of WMRs.

This paper approximates the real robot velocity to the one obtained as the simulation result of sufficiently accurate dynamic model, as was done for the spatial error. Then:

$$V^{real} = V_d \tag{36}$$

The velocity planner fixes an upper bound for the temporal error associated to each posture in this way. The bound is given by a value relative to the time that the path tracker estimates the robot spends in the stationary trajectory, with a relative tolerance t_t^{rel}. Then the following inequality must be satisfied:

$$E_t \leq t_t^{rel} t = t_t^{rel}\frac{S}{V} \tag{37}$$

Let the relative velocity error, e_v, be the relative difference between the robot's real velocity, approximated by simulation outputs, and the velocity of the path tracker:

$$e_v = \frac{V - V_d}{V_d} \tag{38}$$

Therefore, the equation (35) can be rewritten as:

$$E_t = \frac{S}{V}e_v \tag{39}$$

Simulation results from the RAM's dynamic model in Section 2.2., make it possible to express the relative error as a linear function of the velocity, given by:

$$e_v = b_1 V \quad ; \quad b_1 = 4\cdot 10^{-4} V \tag{40}$$

By replacing this function in the calculation of the spatial error in equation (37), a new upper bound for the guide point velocity is found as:

$$V_{Lim4} = \frac{t_t^{rel}}{b_1} \tag{41}$$

where the parameter b_1 must be obtained, offline, from an accurate robot dynamic model.

C. Tip-over limitation. Tip-over occurs when the entire robot weight shifts to one side of the vehicle, and the other wheels are about to lose contact. Thus, the robot is at risk of tipping-over when the reaction force normal to the ground is entirely applied to the outer wheel.[11] The extreme situation, depicted in Figure 6 on a flat terrain, where h is the height of the c.g. of the robot, yields:

$$F_y = F_z\frac{B}{h} \tag{42}$$

By neglecting gyroscope torques, the lateral force, F_y, on flat grounds is simply the centrifugal force and the normal reaction must be the total robot weight. Thus, in order not to surpass the constraint, equation (42) means that the robot velocity must be lower than:

$$V_{Lim5} = \sqrt{\frac{gB}{h}\frac{1}{h|\kappa|}} \tag{43}$$

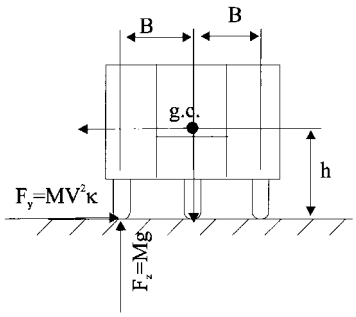

Fig. 6. Tip-over constraint.

https://doi.org/10.1017/S0263574701003770 Published online by Cambridge University Press

where g is the gravity constant. The absolute value makes it possible to free the limitation from the sign of κ.

Different dangerous situations for tipping-over, caused by terrain irregularities or aerodynamic effects are disregarded in indoor navigation. In that case the tip-over constraint should bound the roll and pitch angles of the vehicle.[12]

3.4. Operational constraints

The need for fitting and synchronising the robot's motion with its environment, whether static or dynamic, makes operational constraints necessary.

A. Maximum velocity to avoid collisions. The robot's velocity is limited by a value that assures the robot to stop completely at a distance which is greater than the safety distance, L_{safe}, from any obstacle.[21] This emergency motion should be carry out with the maximum robot deceleration available on non-curved paths, a_b^{max}, a constant calculated later in the paper.

The distance travelled by the robot, moving with velocity V, until it stops, is:

$$s = \frac{V^2}{2a_b^{max}} \tag{44}$$

while the distance covered by the object is:

$$s_{obs} = \frac{V_{obs}}{a_b^{max}} V \tag{45}$$

where V_{obs} is the component of the obstacle velocity towards the robot. When the obstacle motion is completely known, V_{obs} is evident. And when the planner deals with unknown environments, V_{obs} is set as the upper limit of the estimated range of the obstacle velocity, since this constraint does not seek to find optimal motion but rather safe robot motion.

In order to assure that the robot maintains that safe distance, it must comply with the following:

$$s + s_{obs} = D_{obs} - L_{safe} \tag{46}$$

When the planner works in static environments, D_{obs} is the distance from the robot guide point to the obstacle. And for dynamic environments, it is the distance from the robot guide point to the point where the obstacle is detected for the first time, generally equal to the radius of vision of the external sensor system.

By replacing equations (44) and (45) in equation (46), a new upper limit is found for the velocity as:

$$V_{Lim6} = \sqrt{(V_{obs})^2 + 2a_b^{max}(D_{obs} - L_{safe})} - V_{obs} \tag{47}$$

This constraint can be improved taking into account the direction of the spatial path w.r.t. the obstacle. Let θ_{obs} be the orientation of the obstacle boundary on the world frame $\mathcal{F}w$. Then the orientation of the path w.r.t. that boundary is:

$$\theta_{r,obs} = \theta_{obs} - \text{atan}\left(\frac{dY}{dX}\right) \tag{48}$$

and let p_θ be a penalty parameter defined as a piecewise linear function associated to $\theta_{r,obs}$ by arbitrary constants as:

$$p_\theta = \begin{cases} \dfrac{C_{1,1}}{\sin(\theta_{r,obs})} & \ldots\ldots \text{if} \quad \sin(\theta_{r,obs}) > 0 \\ \dfrac{C_{1,2}}{\cos(\theta_{r,obs})} & \ldots\ldots \text{if} \quad \sin(\theta_{r,obs}) \le 0 \end{cases} \tag{49}$$

Then, the constraint is rewritten as:

$$V_{Lim6} = p_\theta\left(\sqrt{(V_{obs})^2 + 2a_b^{max}(D_{obs} - L_{safe})} - V_{obs}\right) \tag{50}$$

when $C_{1,1} = 1$ and $C_{1,2} = 0$, the penalty function is equivalent to bounding the component of the robot's velocity in normal direction towards the obstacle.

B. Maximum approach velocity to the goal point. In the same way and in order to assure safe stopping at the goal point, the algorithm calculates the upper bound function given by:

$$V_{Lim7} = \sqrt{2\, C_2 (S - s) a_b^{max}} \tag{51}$$

where C_2 is an arbitrary constant higher than 1, which reflects a security percentage for stopping and S the total path length.

C. Environmental constraints. A set of velocity constraints which are solely dependent on the robot's working environment can be defined as a function which assigns a maximum speed V_i to each portion of the path, with expressions like:

$$V_{Lim8} = f_{en}(s) = \begin{cases} V_1 & \text{if} \quad 0 \le s \le s_1 \\ \vdots & \\ V_n & \text{if} \quad s_n \le s \le s_{n+1} \end{cases} \tag{52}$$

If the planner deals with dynamic environments, these limits can be formulated in order to avoid those obstacles.[22]

4. ACCELERATION AND DECELERATION CONSTRAINTS

The same constructive, kinematic, dynamic and environmental topics which were analysed for velocity are studied for acceleration in this section.

4.1. Constructive constraints

The maximum allowable torque of tractive and steering motors, $T^t\,|^{max}$ and $T^s\,|^{max}$, and of the braking mechanism, $T^b\,|^{max}$, dictates the maximum torque that can develop at the wheels. Since a tractive/brake motor powers each driven wheel while both steering wheels are linked to a unique servomotor, those limits are given, respectively, by:

$$T_w^t\,|^{max} = \frac{\eta_t}{\xi_t} T^t\,|^{max} \tag{53}$$

$$T_w^s\,|^{max} = \frac{\eta_s}{\xi_s} \frac{T^s\,|^{max}}{2} \tag{54}$$

$$T_w^b\,|^{max} = \frac{\eta_t}{\xi_t} T^b\,|^{max} \tag{55}$$

https://doi.org/10.1017/S0263574701003770 Published online by Cambridge University Press

Where η_t is the efficiency of the drive-train and η_s is the efficiency of the steering-train.

The maximum torques are provided at any velocity by the electric motors assembled on RAM, but this point must be carefully pondered when heat engines are used.

It is worth emphasising that the acceleration capability is not a constructive characteristic of electric motors, when resisting loads are not regarded, hence it is not studied here.

4.2. Constraints forced by the ground

In order to avoid slippage, the maximum effort that the wheel-ground contact can support in the direction j of $\mathcal{F}\ell$, is:

$$F_w^j \mid^{ad} = \mu_j F_w^n \tag{56}$$

The coefficient μ can be assumed to be constant in any direction for uniform rubber wheels if slippage does not occur and terrain characteristics stay uniform. On the other hand the load F_w^n changes with: ground irregularities on 3D terrains, transients of non-stationary manoeuvres, on curved paths, due to lateral load transference produced by the centrifugal force, and on accelerated or decelerated paths, due to longitudinal load transference. The first two phenomena are not very important for navigation in industrial environments,[23] although on bumpy terrains they make another constraint necessary, one which ensures the WMR does not lose contact with the ground.[11]

Regarding the two last phenomena and firstly studying the steering wheels, lateral load transference has no influence, since the wheels are longitudinally aligned with the c.g. of the robot, while the longitudinal load transference due to any acceleration a, yields:

$$\begin{aligned} F_{w1}^n &= F_{w1}^n \mid_0 - \frac{h}{L} Ma \\ F_{w3}^n &= F_{w3}^n \mid_0 + \frac{h}{L} Ma \end{aligned} \tag{57}$$

where $F_{wi}^n \mid_0$ is the static load on i-th wheel. It is evident that the load transference is compensated between both driven wheels, so the total weight available becomes equal to the static load on them. And the maximum lateral effort which can occur from the steering system is, by replacing equation (57) in equation (56):

$$F^s \mid^{ad} = \mu (F_{w1}^n \mid_0 + F_{w3}^n \mid_0) \tag{58}$$

where it is understood that the longitudinal efforts can be neglected in non-driven wheels.

Calling the castor distance d_c, i.e. the longitudinal distance from the rotation axis of the steering system to the wheel centre, the available steering torque limited by the efforts that the wheel-ground contact can support is:

$$T^s \mid^{ad} = \mu d_c (F_{w1}^n \mid_0 + F_{w3}^n \mid_0) \tag{59}$$

For the RAM's driven and braking wheels, because of their location, the normal load is influenced only by centrifugal force, which decreases the weight on the inner wheel and increases it on the outer one, as:

$$\begin{aligned} F_{w2}^n &= F_{w2}^n \mid_0 - \frac{h}{B} MV^2 \kappa \\ F_{w4}^n &= F_{w4}^n \mid_0 + \frac{h}{B} MV^2 \kappa \end{aligned} \tag{60}$$

The transference is also compensated between both wheels. Thus, by replacing equation (60) in equation (56), the longitudinal efforts that the wheel-ground contact of the driven and braking wheels of RAM can support are:

$$\begin{aligned} F^t \mid^{ad} &= \mu (F_{w2}^n \mid_0 + F_{w4}^n \mid_0) \\ F^b \mid^{ad} &= \mu (F_{w2}^n \mid_0 + F_{w4}^n \mid_0) \end{aligned} \tag{61}$$

where it is assumed that lateral efforts on rolling wheels do not significantly reduce their longitudinal friction coefficient.[16]

4.3. Kinematic constraints

As it occurs with velocity, the robot's kinematics would make its guide point acceleration to be a function of the acceleration of the wheels. But, as was argued in Section 4.1, this value is limited exclusively by dynamic capabilities relative to the resisting loads, which are studied in the next section.

4.4. Dynamic constraints

The acceleration or deceleration available for a WMR must be bounded by the results of Sections 4.1. and 4.2.

A. Tractive and braking systems. The maximum acceleration is that which is attained applying the maximum effort when rolling, grade and aerodynamic resistances are overcome. For WMRs aerodynamic resistance is habitually neglected, because of their navigation velocity. Then the maximum acceleration, negotiating a grade j, is:

$$a_{Lim1} = \frac{g}{\gamma} \left(\frac{F_w^x \mid^{max}}{Mg} - f_r \cos [\text{atan}(j/100)] - \sin [\text{atan}(j/100)] \right) \tag{62}$$

where γ is the robot's rotational mass factor and f_r is its coefficient of rolling resistance. $F_w^x \mid^{max}$ is the maximum longitudinal effort, limited either by the motor's power or by the wheel-ground adherence capacity. When $F_L \mid^{max}$ is concerned with the tractive subsystem, a boundary function for acceleration is found, when it is concerned with the braking subsystem, deceleration is constrained. Thus, by introducing the power capacities computed in equations (53) and (55), and the maximum adhesion of equation (61) into the previous equation, the following upper boundary

https://doi.org/10.1017/S0263574701003770 Published online by Cambridge University Press

functions are found for the robot's acceleration and deceleration, respectively:

$$a_{Lim1} = \frac{1}{\gamma M} \cdot \min\left\{ 2\frac{T_w^d \mid^{max}}{R},\ F^t \mid^{ad} \right\} - \frac{g}{\gamma}(f_r \cos[\text{atan}(j/100)] + \sin[\text{atan}(j/100)]) \quad (63)$$

$$ab_{Lim1} = \frac{1}{\gamma M} \cdot \min\left\{ 2\frac{T_w^b \mid^{max}}{R},\ F^d \mid^{ad} \right\} - \frac{g}{\gamma}(f_r \cos[\text{atan}(j/100)] + \sin[\text{atan}(j/100)]) \quad (64)$$

These are constant values as long the coefficient f_r can be considered constant, which occurs when the wheels stay within a small range of their operating variables, the most common situation in WMR motion in industrial environments,[15, 20] where the ground can be assumed of null grade.

B. Steering system. The maximum acceleration of the steering angle can be calculated as:

$$\left| \frac{d^2\delta}{dt^2} \right\|^{max} = \frac{2T_w^2 \mid^{max} - 2 \mid T_{res}^{front} + T_{res}^{rear}}{I_s} \quad (65)$$

where the absolute values free the calculation from the sign of the curvature trajectory.

Looking at the left-hand side of equation (65), it can be expressed by:

$$\frac{d^2\delta}{dt^2} = \frac{d^2s}{d^2t}\frac{d^2\kappa}{ds^2}\frac{d^2\delta}{d\kappa^2} \quad (66)$$

Thus, the acceleration of δ depends on three terms: the acceleration of the trajectory, a; the spatial acceleration of curvature, a characteristic directly derived from the spatial path; and on the last term, which is a characteristic of the robot that can be approximated from its kinematic model equation (1).

Looking at the right-hand side of equation (65): $T_w^s \mid^{max}$ is the maximum steering torque at the wheel, limited either by power, according to equation (54), or by adhesion, according to equation (59); I_s the mass moment of inertia of the whole steering system; T_{front}^{res} and T_{rear}^{res} are the resisting torques at the front and rear wheels.

The last two values can be quantified working with simulation outputs of a successful dynamic model of the robot, as complex as is needed, since computing time is not a problem. Simulation results of the RAM's dynamic model of Section 2.2. make it possible to estimate the sum of the resisting torques in both steering wheels as:

$$\left| T_{res} \right| = \left| T_{res}^{front} + T_{res}^{rear} \right| = \frac{MV^2 \mid \kappa \mid}{2} d_c \quad (67)$$

Thus, the total resisting torque results in a direct ratio to the distribution of the centrifugal force on the wheels that support the vehicle and to the castor distance d_c. A similar result will be found in all robot configurations in which:

- The self-align torques of the wheels are considerably lower than the torques generated by the steering mechanism, i.e., the castor distance is appreciable.
- The robot velocity is not too high, so that the gyroscopic torques at the wheels can be neglected.

By replacing equations (66) and (67) in equation (65) and by isolating the acceleration, a new boundary function is given by:

$$a_{Lim2} = \frac{\min\{2T_w^s \mid^{max}, T^s \mid^{ad}\} - \frac{MV^2 \mid \kappa \mid}{2} d_c}{I_s} \frac{1}{\left| d^2\delta/d\kappa^2 \right|} \frac{1}{\left| d^2\kappa/ds^2 \right|} \quad (68)$$

It can be observed that this upper bound depends on the velocity, which would take the TP to an iteration loop. In order to avoid this costly procedure, V is substituted by the single-valued upper boundary function of velocity, $V_{LIM}(s)$, defined in the next section, making the acceleration boundary even more restrictive.

For RAM, when the quotient $(d^2\delta/d\kappa^2)$ is deduced from its kinematic model, equation (1), the acceleration bound is finally expressed by:

$$a_{Lim2} = \frac{\min\{2T_w^s \mid^{max}, T^s \mid^{ad}\} - \frac{M(V_{LIM})^2 \mid \kappa \mid}{2} d_c}{I_s} \frac{(1 + L^2\kappa^2)^2}{2L^3 \mid \kappa \mid} \frac{1}{\left| d^2\kappa/ds^2 \right|} \quad (69)$$

5. BOUNDARY FUNCTIONS

From all the constraints in Sections 3 and 4, three single-valued functions, parameterised by arc length, s, over the entire spatial path can be generated. They would delimit the permissible region for the robot's guide point velocity, acceleration and deceleration, V_{LIM}, a_{LIM} and ab_{LIM}, respectively.

Assigning the lowest upper bound of each operating variable to each robot position generates the functions. Since all of the constraints are already expressed as a function of the arc length s, the assignment is immediately expressed by:

$$\begin{aligned} V_{LIM}(s) &= \min\{V_{Lim1}(s), V_{Lim2}(s) \ldots V_{Lim8}(s)\} \ \ /s \subset [o, S] \\ a_{LIM}(s) &= \min\{a_{Lim1}(s), a_{Lim2}(s) \ \ /s \subset [o, S] \\ ab_{LIM}(s) &= ab_{Lim1}(s) \ \ /s \subset [o, S] \end{aligned} \quad (70)$$

6. RESULTS

The velocity, acceleration and deceleration constraints have been computed for the path of RAM shown in Figure 7, with high dynamic requirements, which were generated as a cubic spiral in a static environment. The constraints work

https://doi.org/10.1017/S0263574701003770 Published online by Cambridge University Press

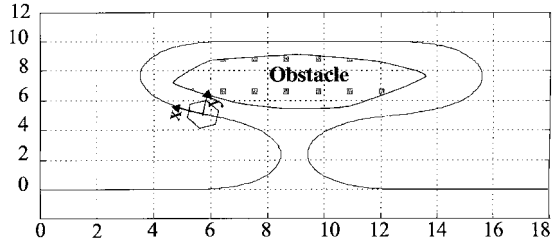

Fig. 7. Spatial path for RAM in a static environment.

with the maximum robot velocity allowed by the performances of their tractive motors equal to 11m/s, whereas the tolerances for the spatial and temporal errors were set to $t_s^{rel}=10\%$ and $t_t^{rel}=10\%$.

The velocity constraints over the entire path are shown in Figure 8. As displayed in Figures 8 and 9, the velocity boundary function, V_{LIM}, is not constant at all. Regarding with the acceleration boundary, it is always dictated by the maximum effort that the wheel-ground contact can support, since the maximum torque of the tractive and steering servomotors are oversize for RAM. Thus, it is a constant function dependent on the wheel-ground adhesion coefficient μ. The same situation was found for the deceleration limit.

When the boundary functions are implemented by a specific velocity planner[24] of WMR, the resulting velocity profile is plotted in Figure 9.

The path tracked by RAM, found as simulation results of its dynamic model, is shown in Figure 10, where the robot spent 8.7s for the task.

If a constant boundary function equated to the minimum of V_{LIM} along the whole path is considered, the total time of the simulated tracked path is 13.8s, 59% higher, but without important reductions of the errors. On the other hand, if the constraints derived from bounding the spatial and temporal errors, $V_{Lim\,3}$ and $V_{Lim\,4}$, are eliminated, the errors of the simulated trajectory are considerably higher, but without significant temporal improvement, only 3.2% time-reduction. Both simulated paths are also in Figure 10.

7. CONCLUSIONS

The work of this paper is applied to the robot RAM, a WMR designed for navigation with high manoeuvrability in indoor and outdoor industrial environments. Thus, its direct and inverse kinematic problem is solved, and a complete dynamic model of the robot, with 12 dof, is developed. The model, aside from retaining all non-linear motions and efforts, pays special attention to the study of wheel-ground interaction. For this purpose, a specific model that computes the contact efforts of homogeneous rubber wheels without profile rolling is researched. It is an analytical model based on experimental measurements of the normal pressure in the contact area of the wheels and on the dynamic efforts found for tyres.

The paper approaches a methodology to identify the region in which velocity, acceleration and deceleration of a WMR must be confined in order to generate a trajectory which is fast, feasible, safe and with low tracking errors. Moreover, this is accomplished evaluating functions that demand low computational cost.

Firstly, the paper deals, on the one hand, with topics related to the performances of steering, tractive and braking subsystems of the autonomous vehicle, as well as mechan-

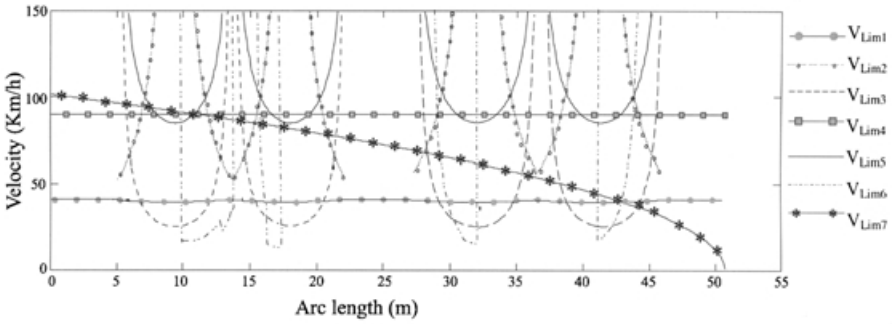

Fig. 8. Velocity boundary functions.

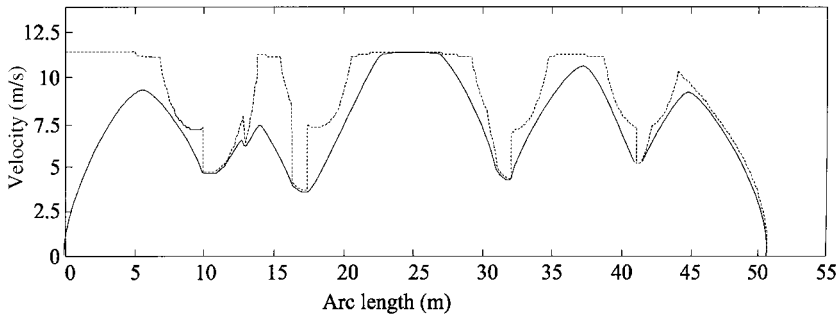

Fig. 9. ——— Velocity profile for the path
------- Velocity boundary function for the path.

https://doi.org/10.1017/S0263574701003770 Published online by Cambridge University Press

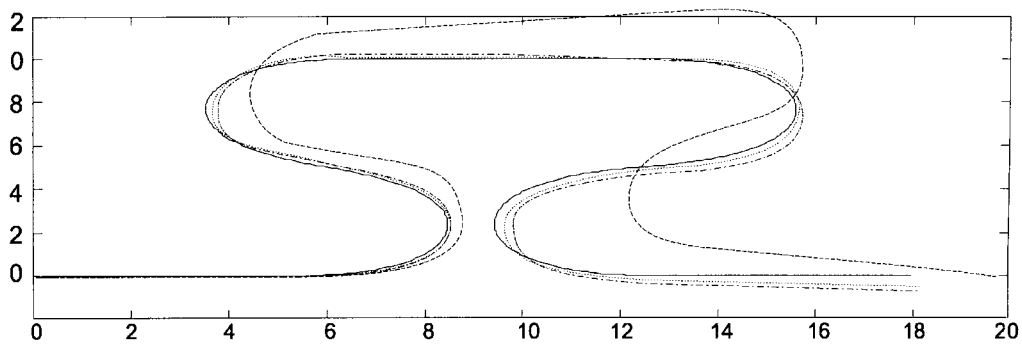

Fig. 10. Simulation results
——— Planned path
–·–·–·– Simulated path with all bounds
····· Simulated path with only the lower bound
--------- Simulated path without spatial and temporal error bounds.

ical properties of the ground. Next the motion capabilities of the robot's guide point are calculated, attending to the kinematics and dynamics of the complete robot system and as functions of the previous results.

The dynamic upper limits for velocity are fixed not only to avoid total vehicle slippage, but also to bound the spatial and temporal errors of a trajectory in which the space path generator and the trajectory tracker work under the kinematic problem solution. This solution considers pure rolling, i.e. it neglects the errors caused by deformations of the wheels and microslippages at the wheel-ground contact area that always exist. The paper estimates the errors from simulation results of a sufficiently accurate dynamic model of the WMR, as complex as is needed since it works offline, so that the computational cost is not increased.

On the other hand, operational constraints, caused by the need for fitting and synchronising the robot's motion with its environment, are also defined.

Finally, the admissible region for velocity, acceleration and deceleration of the robot guide point is delimited by single-valued functions defined by close mathematical forms over the entire spatial path domain. The three functions are computed assigning the lowest upper bound of each operating variable to each spatial position of the robot.

The resulting bounds were included in the TP of the robot RAM, where the constraints were successfully tested by dynamic simulation.

References

1. K. Kant and S. Zucker, "Toward Efficient Trajectory Planning: the Path-Velocity Decomposition", *Int. J. Robotics Research* **2**, No. 3, 72–89. (1986).
2. P.K. Agarwal and H. Wang, "Approximation Algorithms for Curvature-Constrained Shortest Paths", *SIAM J. Computing* **30**, No. 6, 1739–1772 (2001).
3. M.A. Salichs and L. Moreno, "Navigation of Mobile Robots: Open Questions", *Robotica* **18**, Part 3, 227–234 (2000).
4. K.C. Koh and H.S. Cho, "A Smooth Path Tracking Algorithm for Wheeled Mobile Robots with Dynamic Constraints", *J. Intelligent and Robotic Systems* **24**, No. 4, 367–385 (1999).
5. G. Ramírez and S. Zeghloul, "A New Local Path Planner for Nonholonomic Mobile Robot Navigation in Cluttered Environments", *Proc. IEEE Int. Conf. Robotics and Automation* (San Francisco, USA, 2000), pp. 2058–2063.
6. O'Dunlaing, "Motion Planning with Inertial Constraints", *Algorithmica* **2**, 431–475 (1987).
7. K. Fujimura and H. Samet, "A Hierarchical Strategy for Path Planning Among Moving Obstacles", *IEEE Trans. Robotics and Automation* **5**, No. 1, 61–69 (1989).
8. F. Lamiraux, S. Sekhavat and J. Laumond, "Motion Planning and Control for Hilare Pulling a Trailer" *IEEE Trans. Robotics and Automation* **5**, No. 4, 640–652, (1999).
9. W. Weiguo, C. Huitang and W. Peng-Yung, "Optimal Motion Planning for a Wheeled Mobile Robot", *Proc. IEEE Int. Conf. Robotics and Automation* (Michigan, USA, 1999), pp. 41–46.
10. J.S. Choi and B.K. Kim, "Near-Time-Optimal Trajectory Planning for Wheeled Mobile Robots with Translational and Rotational Sections", *IEEE Trans. Robotics and Automation* **17**, No. 1, 85–90 (2001).
11. Z. Shiller, "Motion Planning for Mars Rover", *Proc. I Workshop Robot Motion and Control* (1999), pp. 257–262.
12. M. Cherif, "Motion Planning for All-Terrain Vehicles: A Physical Modelling Approach for Coping with Dynamic and Contact Interaction Constraints", *IEEE Trans. Robotics and Automation* **15**, No. 2, 202–218 (1999).
13. A. Ollero, A. Simón, F. Garcia and V. Torres, "Integrated Mechanical Design and Modelling of a New Mobile Robot". In: *Intelligent Components and Instruments for Control and Applications* (Pergamon Press, USA, 1993), pp. 461–467.
14. M. Prado, "Dynamic Modelling of Mobile Robots. Application to Trajectory Planning", *PhD Thesis* (University of Málaga, Málaga, Spain, 2000, in Spanish).
15. A. Gentile, A. Messina and A. Trentadue, "Dynamic Behaviour of a Mobile Robot Vehicle with a Two Caster and Two Driving Wheel Configuration", *Vehicle System Dynamics* **25**, 89–112 (1996).
16. H. Dugoff, P.S. Fancher and L. Segel, "An analysis of Tire Properties and Their Influence on Vehicle Dynamic Performance", *SAE Trans. Paper 700376* (1970).
17. A. Pérez, M. Prado and A. Simón, "High Resolution System for Measurement of Contact Pressure of Commercial Tires", *Proc. XIV Congreso Nacional de Ingeniería Mecánica* (Madrid, Spain, 2000, in Spanish), pp. 367–375.
18. H.B. Pacejka and L. Besselink, "Magic Formula Tyre Model with Transient Properties", *Vehicle System Dynamics* **27**, sup., 234–246 (1997).
19. A. Alloum, "Vehicle Modelling Aspects for an Embedded Real-Time Application", *Vehicle System Dynamics* **27**, 187–219 (1997).
20. J.I. Wong, *Theory of Ground Vehicles* (John Wiley & Sons, USA, 1993).
21. J. Miura and Y. Shirai, "Modelling Motion Uncertainty of Moving Obstacles for Robot Motion Planning", *Proc. IEEE Int. Conf. Robotics and Automation* (San Francisco, USA, 2000), pp. 2258–2263.

https://doi.org/10.1017/S0263574701003770 Published online by Cambridge University Press

22. V. Lumelsky and S. Tiwari, "Velocity bounds for motion planning in the presence of moving planar obstacles", *Proc. IEEE/RSJ/GI Int. Conf. Intelligent Robots and Systems* **3**, 1914–1921 (1994).
23. Kelly and A. Stentz, "Analysis of Requirements for High Speed Rough Terrain Autonomous Mobility. Part 1: Throughput and Response" *Proc. IEEE Int. Conf. Robotics and Automation* (Albuquerque, USA, 1998), pp. 3318–3325.
24. V. Muñoz, A. Ollero, M. Prado and A. Simón, "Mobile Robot Trajectory Planning with Dynamic and Kinematic Constraints", *Proc. IEEE Int. Conf. Robotics and Automation* **4** (San Francisco, USA, 1994), **Vol. 4**, pp. 2802–2807.

https://doi.org/10.1017/S0263574701003770 Published online by Cambridge University Press